01 Apr 2022

Quantitative Evaluation of Steel Corrosion Induced Deterioration in Rubber Concrete by Integrating Ultrasonic Testing, Machine Learning and Mesoscale Simulation

Jinrui Zhang

Mengxi Zhang

Biqin Dong

Hongyan Ma
Missouri University of Science and Technology, mahon@mst.edu

Recommended Citation

J. Zhang et al., "Quantitative Evaluation of Steel Corrosion Induced Deterioration in Rubber Concrete by Integrating Ultrasonic Testing, Machine Learning and Mesoscale Simulation," *Cement and Concrete Composites*, vol. 128, article no. 104426, Elsevier, Apr 2022.
The definitive version is available at https://doi.org/10.1016/j.cemconcomp.2022.104426

Cement and Concrete Composites 128 (2022) 104426

Contents lists available at ScienceDirect

Cement and Concrete Composites

journal homepage: www.elsevier.com/locate/cemconcomp

Quantitative evaluation of steel corrosion induced deterioration in rubber concrete by integrating ultrasonic testing, machine learning and mesoscale simulation

Jinrui Zhang [a], Mengxi Zhang [a,*], Biqin Dong [b], Hongyan Ma [c]

[a] State Key Laboratory of Hydraulic Engineering Simulation and Safety, Tianjin University, Tianjin, 300350, China
[b] Guangdong Province Key Laboratory of Durability for Marine Civil Engineering, Shenzhen University, Shenzhen, 518060, China
[c] Department of Civil, Architectural and Environmental Engineering, Missouri University of Science and Technology, Rolla, MO, 65409, USA

ARTICLE INFO

Keywords:
Rubber concrete
Corrosion degree
Ultrasonic signals
Machine learning
Robustness validation
Mesoscale simulation

ABSTRACT

Chloride-induced steel corrosion seriously affects the durability of reinforced concrete structures. Rubber concrete, an environmentally friendly construction material in which waste rubber is recycled as a concrete component, has demonstrated superior resistance to chloride-induced steel corrosion and the subsequent concrete deterioration. However, quantitative evaluation of the degree of deterioration in rubber concrete based on nondestructive detection is challenging due to the complexity of the material. In this paper, reinforced concrete specimens with rubber contents of 0, 10% and 20% are subjected to the electrochemically accelerated corrosion experiments and monitored by ultrasonic testing. Six machine learning models are trained by the data derived from the ultrasonic testing to predict the corrosion degree based on ultrasonic traits. The results show that the machine learning models except for the linear model can accurately and robustly predict the corrosion degree under the interference of outlier amplitude and size of training set. Furthermore, the corrosion-induced deterioration process is computed by mesoscale simulation based on the corrosion degree, so that the damages of specimens with different rubber contents are quantitatively evaluated. The experimental and computational studies prove that the addition of rubber into concrete effectively retards the corrosion of steel and the deterioration of concrete.

1. Introduction

The durability of reinforced concrete structures is a major concern for the designers and operators of civil infrastructure. When exposed to marine environment, the reinforced concrete structures become vulnerable due to chloride-induced steel corrosion [1–3]. Corrosion occurred on the surface of the steel rebar expands over time and further results in deterioration and cracking of the concrete cover. The corresponding maintenance process is time-consuming and costly. For instance, in 2014, the total cost of corrosion in China was estimated to be CNY 2127.8 billion. Thus, it is an urgent problem to resist chloride diffusion and prevent the steel corrosion and its resultant deterioration in infrastructure exposed to marine environment.

As an environmentally friendly construction material developed from recycling of waste rubber, rubber concrete (RC) has been shown to be corrosion-resistant [4]. The mechanisms of this merit may include improved chloride penetration resistance (because the chloride ions can be confined in rubber chains during their penetration process [5]), increased electrical resistance of concrete, smaller expansion resulted from a specific extent of corrosion and improved cracking resistance of concrete [6,7]. In the past few decades, researchers mainly focused on the properties of chloride ions transportation in rubber concrete [8,9]. The corrosion inhibition mechanisms were also revealed by means of experiments. However, steel corrosion in reinforced concrete is normally concealed, and in most cases, it could lead to cracking, spalling and delamination of the concrete cover. For the prestressed concrete structures, the corrosion of the steel wires may even lead to brittle failure and possible sudden collapse. To secure marine infrastructure and promote the application of rubber concrete in marine environment, it is of great significance to monitor the corrosion degree of rebar (so to generate warning before catastrophic cumulation of corrosion) and quantitatively evaluate the deterioration degree of concrete considering

* Corresponding author.
E-mail address: zhangmx@tju.edu.cn (M. Zhang).

https://doi.org/10.1016/j.cemconcomp.2022.104426
Received 29 June 2021; Received in revised form 23 January 2022; Accepted 26 January 2022
Available online 3 February 2022

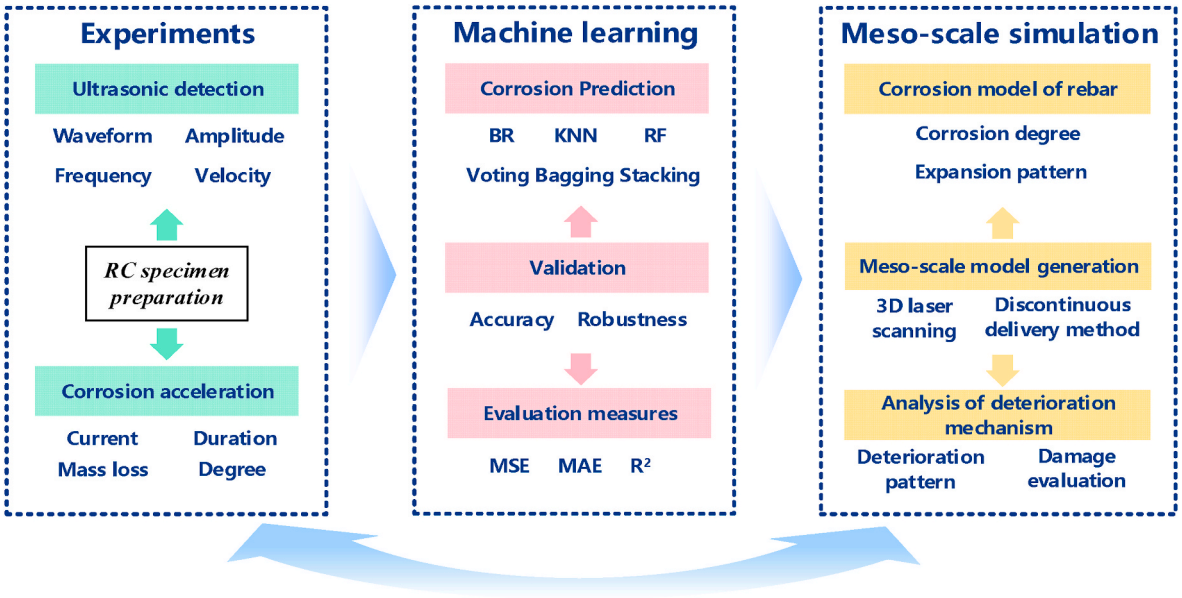

Fig. 1. Methodology framework of this study.

the incorporation of rubber.

There are three main methods for estimating and predicting the extent of steel corrosion in concrete structures, namely, empirical methods, reaction control methods, and electrochemical methods. The empirical method assumes a direct relationship between corrosion rate and basic structural parameters such as water-to-cement ratio, chloride content, temperature, and relative humidity [10–12]. The reaction control method (quasi-empirical) considers the change of physical monitoring indicators (e.g., electrical resistivity, oxygen diffusion resistance, and electromagnetic properties) before and after corrosion of reinforced concrete [13,14]. The above two methods are relatively simple and convenient for engineers to operate, but the complicated relationship between physical monitoring indicators and corrosion degree cannot be represented accurately. The electrochemical methods can reflect the corrosion mechanism as comprehensively as possible [15,16], but not as convenient as the other two types of methods when used in practice. Nondestructive testing methods, including measurements of physico-mechanical and electrochemical parameters, have been widely adopted to monitor the corrosion state of reinforcement in concrete in laboratories and field [17–20]. Ultrasonic testing is a well-developed nondestructive testing method, with strong penetrating ability to medium. To detect the subtle changes of concrete structures that cannot be recognized by direct waves, advanced methods (e.g., coda wave) could be adopted to accurately monitor the behaviors of concrete [21,22]. A critical issue of nondestructive tests is that they normally test a single variable which is tied (linearly or non-linearly) to the target performance, which is often arbitrary, unreliable, or case-dependent (when conventional data interpretation methods are used). Therefore, it is highly desirable to establish advanced data-processing methods and quantitative evaluation methods based on nondestructive tests in consideration of convenience and reliability for monitoring of corrosion-induced deterioration of concrete.

Machine learning (ML) algorithms, supported by a large amount of data, can accurately express the nonlinear relationship between variables. ML has been successfully applied to the evaluation and prediction of concrete properties. Zhang et al. [23] and Cook et al. [24] predicted mechanical properties (e.g., compressive strength) of hydraulic concrete by ML algorithms, and the influences of mix proportion and curing conditions on mechanical properties are analyzed and validated quantitatively. Cai et al. [25] adopted ensemble ML to predict the surface chloride concentration of concrete in marine environment. ML also shows good applicability in solving problems of image identification, construction quality monitoring of dam [26], construction productivity evaluation [27] and so on. In the field of nondestructive testing (nondestructive testing, NDT), Zhang, et al. [28] coupled continuous wavelet transform and machine learning to detect the onset of ultrasonic signals obtained from the test of concrete piles. The favorable performance of these methods shows the effectiveness and feasibility of interpreting data from NDTs with machine learning to improve their reliability.

When it comes to post-corrosion deterioration of reinforced concrete, repeatable numerical simulations that can supplement the results of experiments have become an important class of methodologies [29,30]. Gebreyouhannes and Maekawa [31] simulated the corrosion profile considering the formation and migration of corrosion products. Kuntal et al. [32] integrated the technique of Model Predictive Control (MPC) with Rigid-Body-Spring Models (RBSM) for the simulation of corrosion-induced cracking in concrete. However, during the process of macro-scale simulation, the concrete was often assumed as a homogeneous continuous medium which deviate from the heterogeneous nature of concrete. Mesoscopic simulation is therefore desired for more accurate evaluations of concrete deterioration induced by steel corrosion.

At present, mesoscale simulations of concrete can be conducted following either continuous medium or discontinuous medium methods. Based on various damage constitutions, the continuum simulation methods assume concrete to be a multiphase composite material composed of aggregates, mortar, interfacial transition zone (ITZ) and gaps. The constitutions mesoscopic model can be established in the following two manners: (1) The accurate realistic mesoscopic model, constructed based on XCT scanning [33,34], which is difficult to be widely used due to its high cost; and (2) The simplified high-efficiency mesoscopic models, constructed based on various simplified aggregate delivery algorithms [35,36]. In the simplified models, the aggregate is spherical, ellipsoidal or polyhedral, which cannot reflect the true shape of aggregate and its refinement degree is not high. The discontinuous medium methods assume that the concrete mortar and aggregate are composed of several rigid spherical particles with different sizes. This method is mainly used to simulate the flow, compaction, aggregate crushing and irregular movement of fresh concrete [37,38]. A large number of particles are needed to preset before the discontinuous mesoscale simulation of concrete, which is inefficient in calculation and difficult in parameter calibration. It is a great challenge to ensure the

Table 1
Mix proportions of RC (kg/m^3).

NO.	Cement	Rubber	Sand	Coarse aggregate	Water
PC	337	0	506	607	135
RC10		37	455		
RC20		74	405		

solution accuracy and calculation efficiency simultaneously.

The literature review has revealed the scientific significance and engineering value for developing a quantitative method to characterize the corrosion of steel bars and evaluate the deterioration of rubber concrete, which has high accuracy and can be used for on-site nondestructive testing of reinforced concrete structure. In this paper, concrete specimens with various rubber contents, reinforced by steel rebar, are prepared and subjected to electrochemically accelerated corrosion. Ultrasonic technology is employed to monitor the steel corrosion and potential deterioration of concrete and extract degradation indicators, since it has been proven to be capable of evaluating concrete damage and cracks caused by corrosion of steel bars [39–42]. The ultrasonic parameters (e.g., amplitude and velocity), concrete mixture parameters (e.g., rubber content), and steel corrosion parameters (e.g., corrosion current and mass loss) are taken from experimental measurements to form a database, based on which machine learning prediction models for the corrosion degree of steel bar are trained and validated. The performances of six machine learning models are compared from the view of accuracy and robustness to select the favorable corrosion degree prediction model. Finally, to investigate the deterioration mechanism of rubber concrete, a micro-element volume fraction method, which can describe the geometric characteristics of real aggregate, is informed by the degree of steel corrosion (predicted by the machine learning model) and used for the refinement simulation of steel corrosion induced concrete deterioration at the mesoscopic scale. The overall methodology framework of this study and how various components are integrated are illustrated in Fig. 1.

2. Methodology

2.1. Experiments and data collection

2.1.1. Specimen preparation

Table 1 lists the mixture proportions of plain concrete (PC) and rubber concrete (RC). RC10 and RC20 refer to the rubber concrete with rubber replacing 10% and 20% of sand volume. Ordinary portland cement which meets the requirements of the ASTM C150 Type I was used as the cementitious material in the production of PC and RC. The fineness modulus of the selected sand is 2.6. In addition, Table 2 illustrates components of rubber particles adopted in the experiments. The apparent density of the rubber is 1050 kg/m^3 and the diameter of over 80% rubber particles is in the range of 1–2 mm as shown in Fig. 2. The gradation of coarse aggregate is given in Table 3. In addition, Q235 ribbed steel bars with a diameter of 14 mm are set in the center of prism specimens poured by PC and RC. Mechanical vibration is selected for forming specimens with the size of 100 × 100 × 400 mm. These specimens are demolded after 24 h, and then cured for 28 days at controlled temperature 20 ± 5 °C and relative humidity 95%.

2.1.2. Data collection techniques

The electrically accelerated corrosion test is a method to simulate the corrosion of steel bars under natural conditions, which can greatly accelerate the corrosion rate [43,44]. After the curing of specimens, the electrically accelerated corrosion test is carried out and the circuit of this test is connected as shown in Fig. 3. In this case, the steel bar plays the role of the anode and the copper rod is used as the cathode. Part of the specimen (20 mm below the bare steel bars) is infiltrated into 3.5% NaCl solution, which is necessary to ensure the de-passivation of steel bar. The accelerated corrosion process is realized by direct-current stabilized power supply with the adjustment range of input 0 ~ 30V and 0 ~ 5A. The selected voltage for each specimen is a constant at 30 V to provide the same corrosion environment to explain the influence of rubber content on corrosion resistance. In addition, the total power-on duration is 450 h and the current is monitored in real time.

As an NDT, ultrasonic testing has been used to investigate the

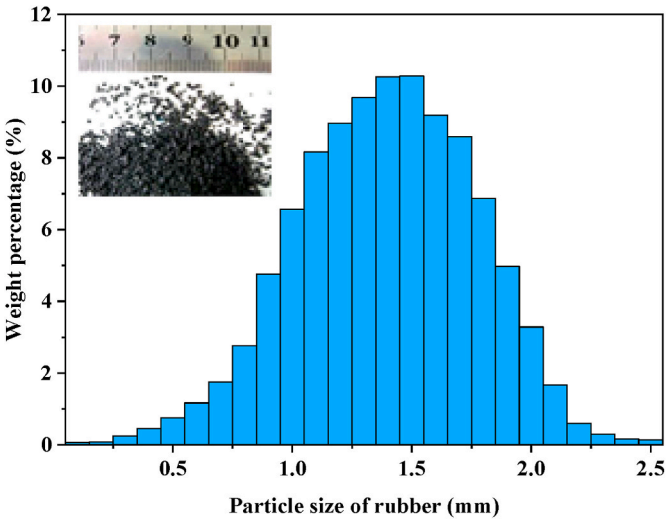

Fig. 2. Morphology and particle size distribution of rubber.

Table 3
Gradation of the coarse aggregate.

Sieve size (mm)	Sieve residue (%)	Accumulative sieve residue (%)
26.5	0.51	0.51
19	28.97	29.48
16	22.86	52.34
9.5	34.5	86.84
4.75	12.24	99.08
<4.75	0.46	99.54

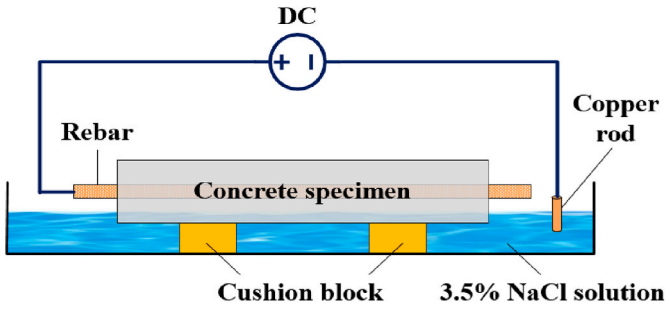

Fig. 3. Schematic of electrochemical accelerated experiment.

Table 2
Components of rubber (%).

Rubber hydrocarbon	Carbon black	Acetone extract	Isoprene	Ash	Water	Fiber	Metal	Others
45.2	25.8	14.2	12.1	0.9	0.8	0.5	0.08	0.42

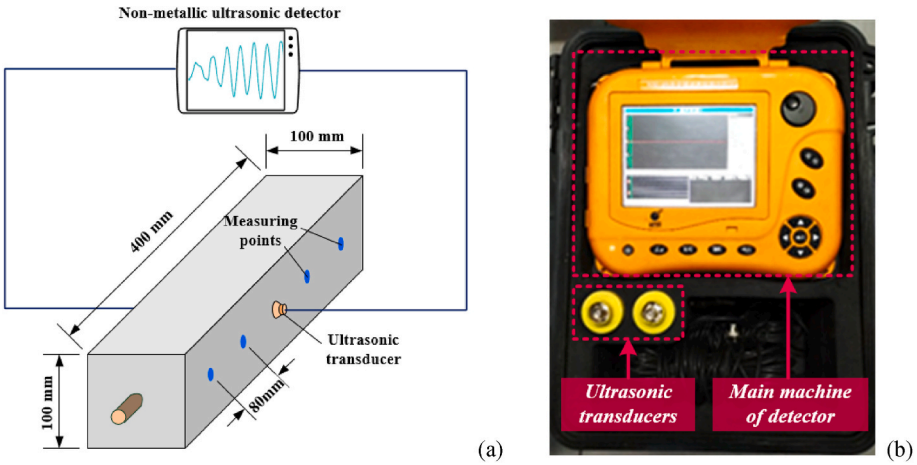

Fig. 4. The diagram of ultrasonic testing. (a) Arrangement of measuring points (b) Non-metallic ultrasonic detector.

Table 4
The parameters of different prediction models.

Model	Parameters	Value	Model	Estimators
Bayesian Ridge	n_iter	1000	Voting/ Bagging	Meta-estimator1: Random Forest-1
	α_1, α_2	10^{-6}		Meta-estimator2: Random Forest-2
	λ_1, λ_2	10^{-6}		Meta-estimator3: K Nearest Neighbors-1
	normalize	True		Meta-estimator4: K Nearest Neighbors-2
	verbose	True		Meta-estimator5: Gaussian Processes
K Nearest Neighbors	n_neighbors	5	Stacking	Meta-estimator1: Random Forest-1
	leaf_size	30		Meta-estimator2: Random Forest-2
	metric	minkowski		Meta-estimator3: K Nearest Neighbors-1
Random Forest	n_estimators	100		Meta-estimator4: K Nearest Neighbors-2
	min_samples_split	2		Meta-estimator5: Gaussian Processes
	max_features	auto		Final-estimator: Gradient Boosting

Table 5
The description of collected data.

Data type	Variable name	Unit	Minimum	Maximum	Average
Input	Amplitude	dB	37.96	109.3	67.69
	Velocity	km/s	0.80	4.63	2.81
	Rubber content	%	0	20	–
Output	Mass loss	g	0	39.26	13.09

structural properties of various materials in real time in engineering [45–48]. Ultrasonic transmission method was used to detect the corrosion degree of rebar in the specimens during the process of accelerated corrosion. The measuring points, located in the middle of prism specimen, were arranged at equal intervals of 80 mm as shown in Fig. 4 (a). Phenyl salicylate was adopted as the coupling agent to adhere the transducers to the measuring points on the surface of specimen. The

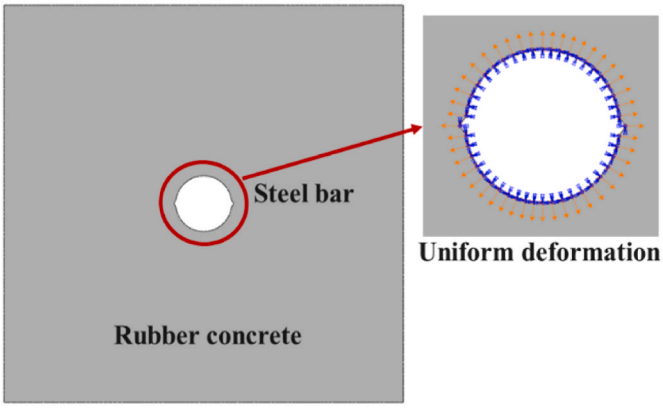

Fig. 5. Chloride-induced uniform corrosion expansion.

transmission voltage and frequency of non-metallic ultrasonic detector, shown in Fig. 4 (b), were adjusted to 500 V and 50 kHz, respectively. The amplitude and velocity of ultrasonic were obtained at multiple time points during the range of 0–450 h.

2.1.3. Data processing

Continuous Wavelet Transform (CWT) can produce a time-frequency representation with high resolution. For a given mother wavelet ψ, the CWT of $x(t)$ at scale a and time shift b is given by

$$W_x(a,b) = \frac{1}{\sqrt{a}} \int_{-\infty}^{\infty} x(t)\psi^* \left(\frac{t-b}{a}\right) dt \quad (1)$$

where, the * is the complex conjugate, $W_x(a,b)$ is the wavelet coefficient representing of $x(t)$. Then the frequency of sampled ultrasonic signals can be obtained according to the wavelet coefficient.

Mass loss can be used to represent the corrosion degree of steel bar at the laboratory level. According to Faraday's law, the mass loss of steel corrosion could be estimated by the weight of the steel oxidized by the electric charge of steel bar by:

$$M_{loss} = T_C \times \frac{E_W}{F} = \int_{t_s}^{t_e} i(t)dt \times \frac{E_W}{F} \quad (2)$$

where M_{loss} refers to the total mass loss for the steel bar (g), T_C refers to the total quantity of electric charge, which could be expressed as an integral form of current $i(t)$ versus time (from start time t_i to end timet_e). The equivalent weight E_W of carbon steel is 27.93 g/mol and the Faraday

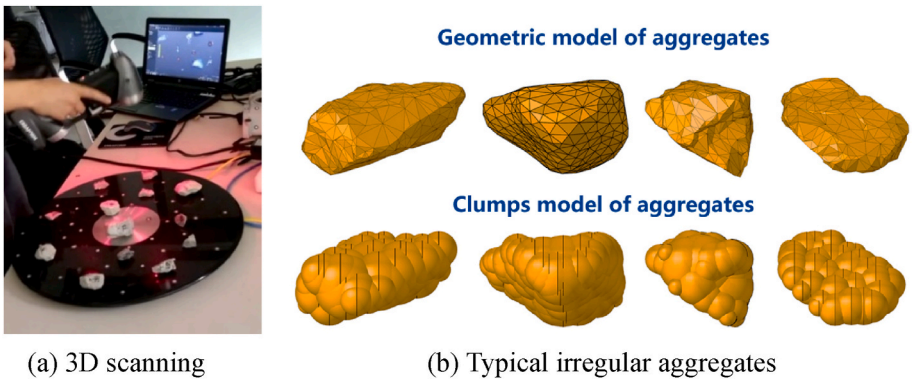

Fig. 6. 3D scanning and selected aggregates.

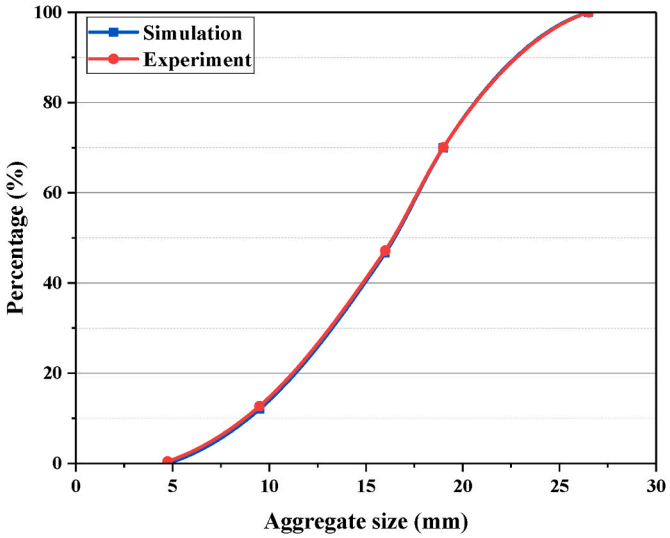

Fig. 7. Gradation curve of aggregates.

Table 6
The description of collected data.

Rubber content (%)	Corrosion degree ρ (%)	Corrosion expansion thickness (mm)
0	13.35	0.868
10	11.05	0.732
20	7.57	0.511

constant F adopted in this study is 96494 A · s/mol. It is assumed that the current efficiency is 100%, which may be slightly different to the efficiency of actual situation, which is lower than 100% initial stage and higher than 100% in the later stage of accelerated corrosion experiment [15].

2.2. Machine learning models

2.2.1. Models and parameters

This section briefly introduces six machine learning models, which have been implemented in this study, including three standalone models and three ensemble models. These algorithms can effectively use the large number of data collected in Section 2.1. (1) Bayesian ridge (BR) regression is a linear model. The predicted value is considered as a linear combination of input variables. To avoid multicollinearity of least squares regression, a penalty coefficient is imposed in the ridge regression. (2) *K* nearest neighbor (KNN) assumes that training data samples are represented by N-dimensional attributes, and training samples can be represented as a series of point sets in N-dimensional space [27]. The *K* nearest neighbor is measured by the Euclidean Distance or other distance of the spatial sample points. (3) Random forest: the core idea of random forest is to combine multiple weak regression trees into a forest by using certain rules, and realize cumulative effect by integrating multiple evaluators. In this way, the accuracy of tree models can be improved and the phenomenon of over-fitting can be effectively avoided [28]. (4) The other three methods, voting, bagging and stacking, are typical strategies of ensemble machine learning. The target of ensemble methods is to combine several meta estimators constructed by a given learning algorithm in order to improve the generalization ability or robustness over a single estimator. The above regression model is established by coding based on Scikit-learn, which is a free machine learning library for the Python programming language [49]. Further details and the optimum parameters of various machine learning models are provided in Table 4 and Supplementary Information 1.

A total of 837 structured data, which can be properly processed by machine learning method, were collected from PC and RC specimens by the above experiment methods as shown in Supplementary Information 2. The machine learning models is effective and suitable when dealing with regression of structured data, which has been proved by the research of our team (see reference [23,27–29]). Thus, 80% of the raw data is selected randomly to train the machine learning models and the rest is selected as the testing set to verify the accuracy of the models. The input and output variables of machine learning models are listed in Table 5. The features of each measured ultrasonic (Amplitude and Velocity) corresponds to a calculated mass loss. It is worth noting that all

Table 7
Material mechanical properties.

Rubber content (%)	Rubber mortar			Aggregate	Interface transition zone		
	Elastic modulus (GPa)	Tensile strength (MPa)	Compressive strength (MPa)	Elastic modulus (GPa)	Initial stiffness (GPa/mm)	Tensile strength (MPa)	Fracture energy (N/mm)
0	40.80	3.15	43.70	50	32.64	2.80	0.0013
10	27.80	2.58	30.50		22.24	2.30	
20	23.92	2.14	21.60		19.14	1.90	

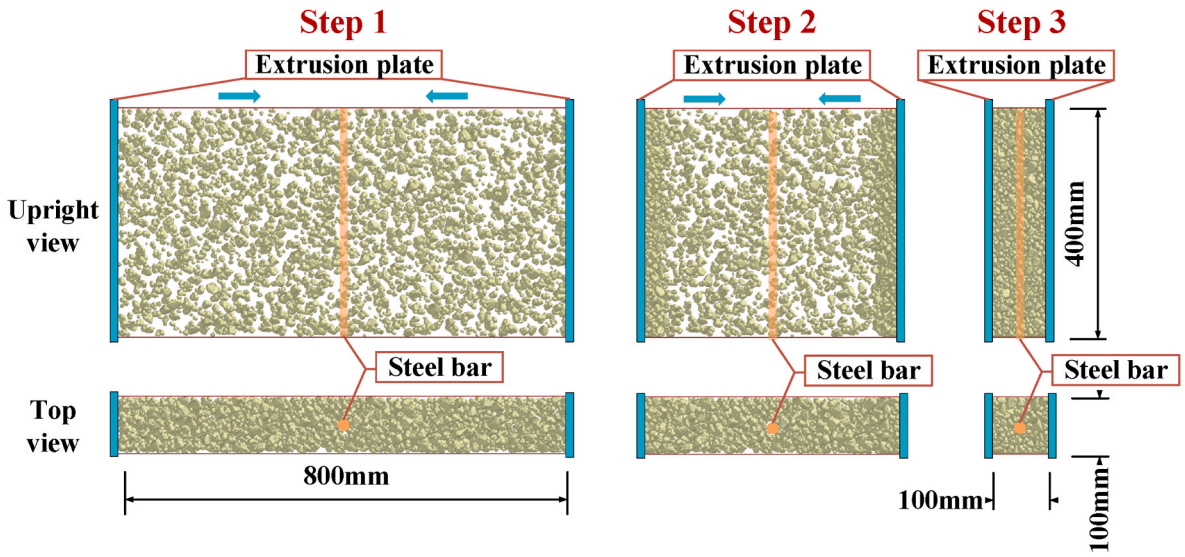

Fig. 8. Generation process of irregular aggregate in rubber concrete specimen.

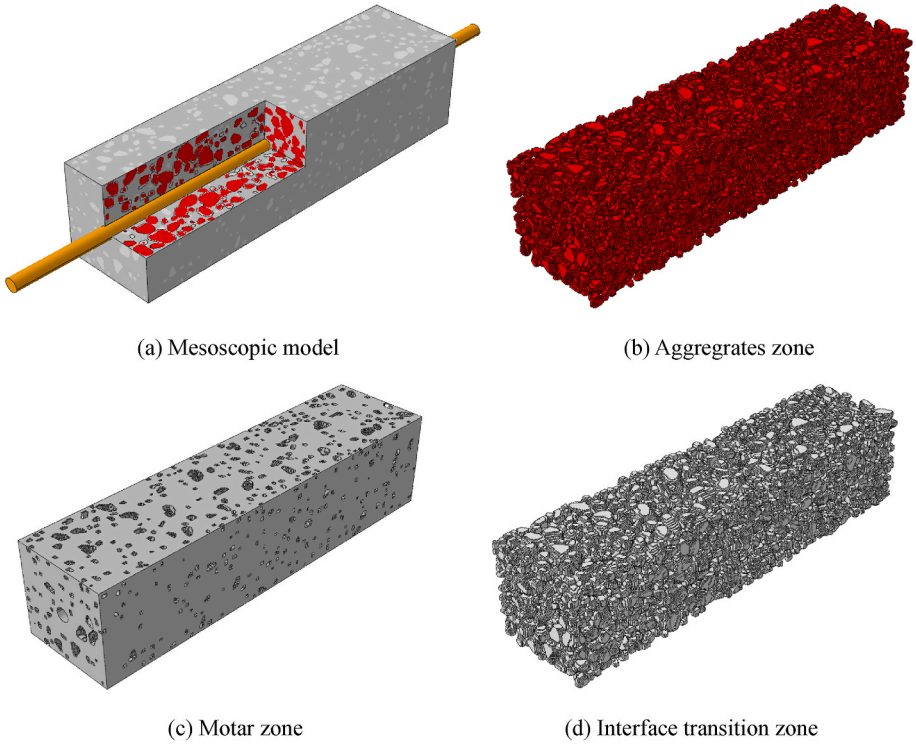

Fig. 9. 3D mesoscale model of rubber concrete specimen.

the input variables vary widely, indicating that these indicators can be adopted to machine learning models to reflect the corrosion state in this study.

2.2.2. Evaluation measures

The prediction accuracy of machine learning models was evaluated according to mean absolute error (*MAE*), mean squared error (*MSE*) and determination coefficient (R^2), these measures can be calculated by the following formulas:

$$MAE = \frac{1}{N}\sum_{i=1}^{N}|y - y'| \tag{3}$$

$$MSE = \frac{1}{N}\sum_{i=1}^{N}(y - y')^2 \tag{4}$$

$$R^2 = 1 - \frac{\sum_{i=1}^{N}(y - y')^2}{\sum_{i=1}^{N}(y - \bar{y})^2} \tag{5}$$

where y refers to the actual value, y' represents the predicted value and $\bar{y}$ represents the average of the actual value. N refers to the size of testing set.

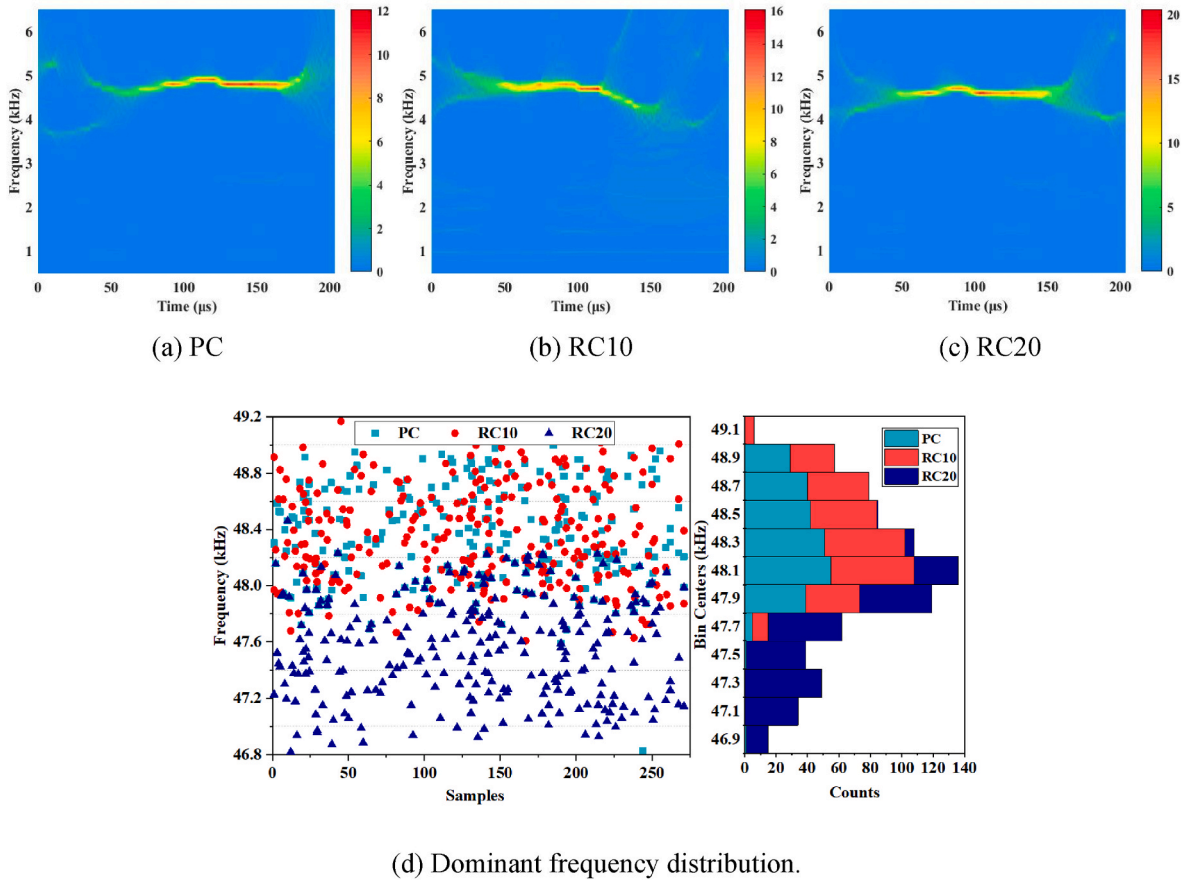

Fig. 10. Time-frequency and frequency distribution diagrams.

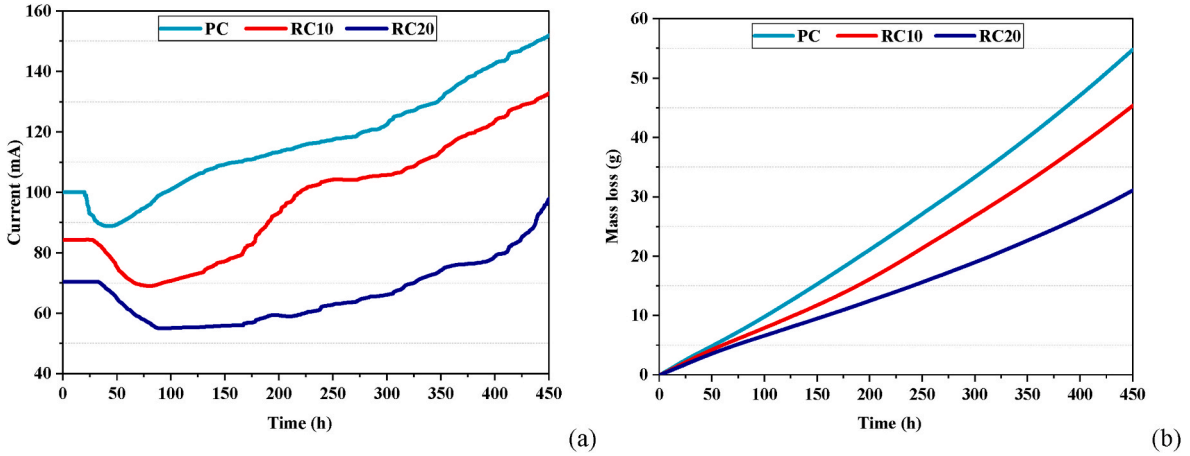

Fig. 11. Changing process of corrosion current and mass loss. (a) Corrosion current (b) Mass loss.

2.3. Mesoscale simulation of corrosion-induced deterioration

2.3.1. Expansion model of corrosion products

Corrosion rust progression around the reinforcement in concrete can be represented by various models such as non-uniform corrosion model, quadratic semicircle model, partly uniform model and so on [50,51]. According to the experiment section, the steel bars ($D = 14$ mm) are set in the center of prism specimens produced by PC and RC. Therefore, in this paper, it is assumed that the volumetric expansion of steel bars caused by corrosion products is uniform as shown in Fig. 5. The total volume per unit length of the corrosion products V_r and the corroded part of the steel bar V_s can be represent as formula (6) - (9), respectively [52].

$$V_r = V_{r1} + V_{r2} \tag{6}$$

$$V_s = V_{s1} + V_{s2} \tag{7}$$

$$V_{r1} = 2\pi\delta_0 + V_{s1} \tag{8}$$

$$V_{r2} = V_c + V_{s2} \tag{9}$$

where subscript 1 and 2 represent the volume changing at the stage of

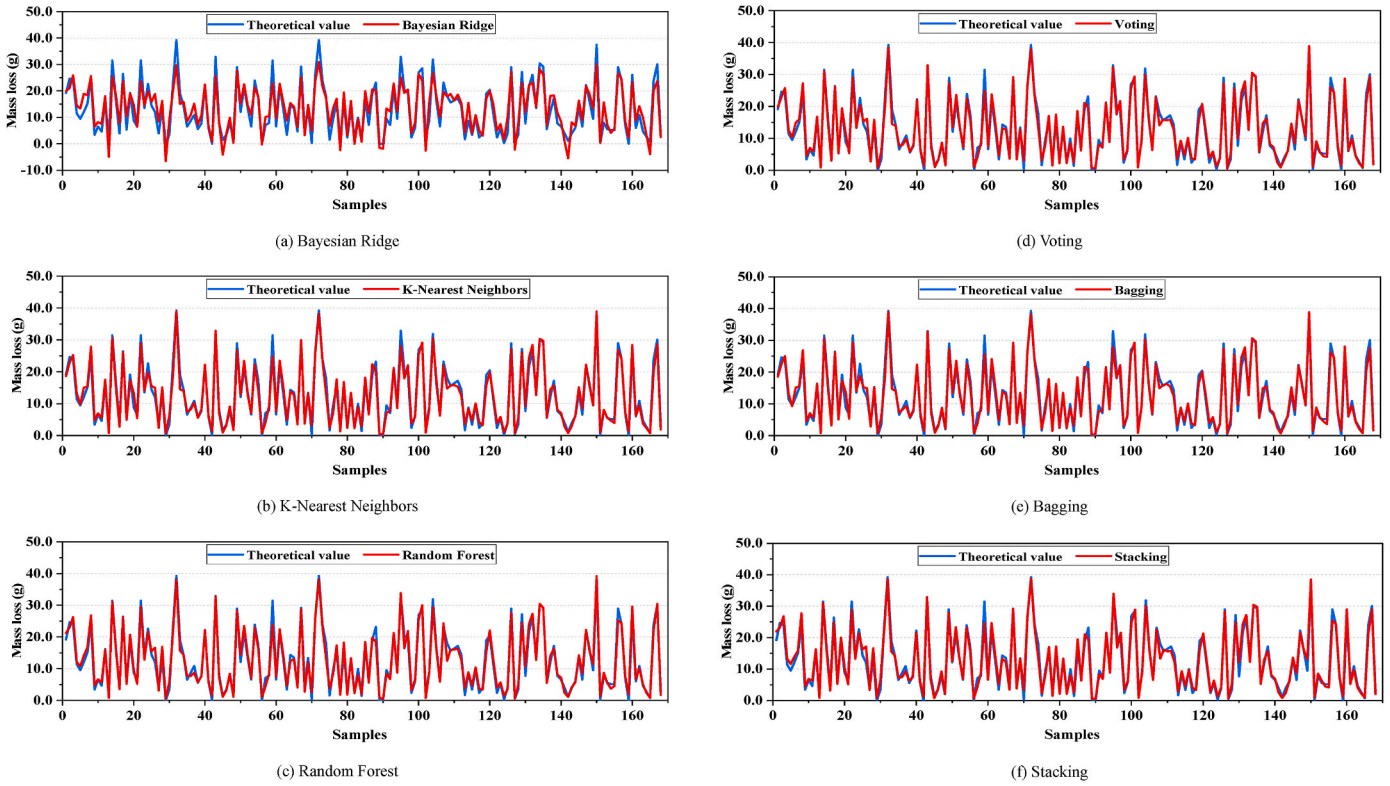

Fig. 12. Theoretical versus predicted mass loss results of ML models.

Table 8
Results of evaluation measures of ML models.

	R^2	*MAE* (g)	*MSE* (g^2)
BR	0.867	2.893	12.735
KNN	0.970	1.256	2.880
RF	0.971	1.221	2.820
Voting	**0.974**	**1.176**	**2.431**
Bagging	0.972	1.221	2.706
Stacking	0.973	1.220	2.781

*Highlighted in bold means the best performance measure of data mining model.

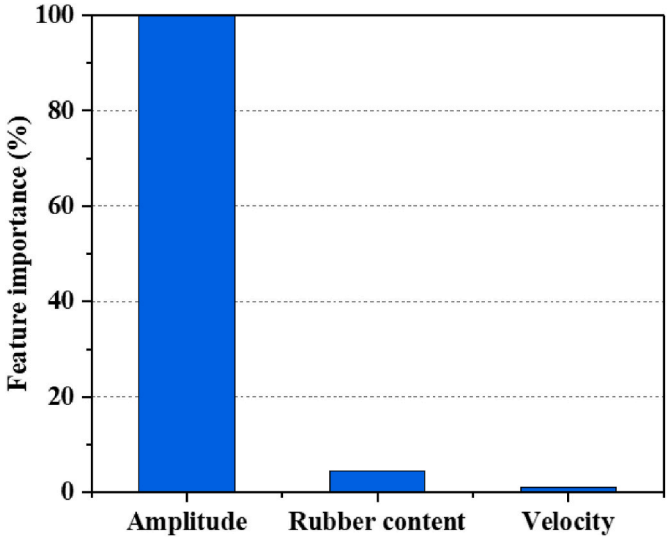

Fig. 13. Feature importance of input variables.

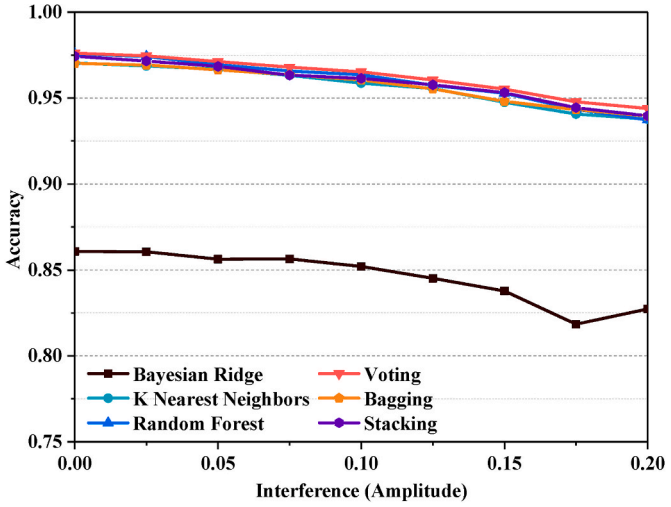

Fig. 14. The prediction accuracy versus interference of ML models.

free expansion and stress initiation, respectively. δ_0 is the thickness of the interfacial layer between steel bar and concrete. V_c is the expansion volume of the surrounding concrete per unit length. The relationship between V_r and V_s can be described as following.

$$V_r = nV_s \tag{10}$$

where $n = 3$ is selected as the ratio of volume expansion of corrosion products [53]. V_s can be obtained by connecting formula (6) – (10). In addition, the corrosion degree ρ represent the percentage of steel mass loss to the original steel mass.

$$\rho = \frac{V_s}{\pi R^2} \times 100\% \tag{11}$$

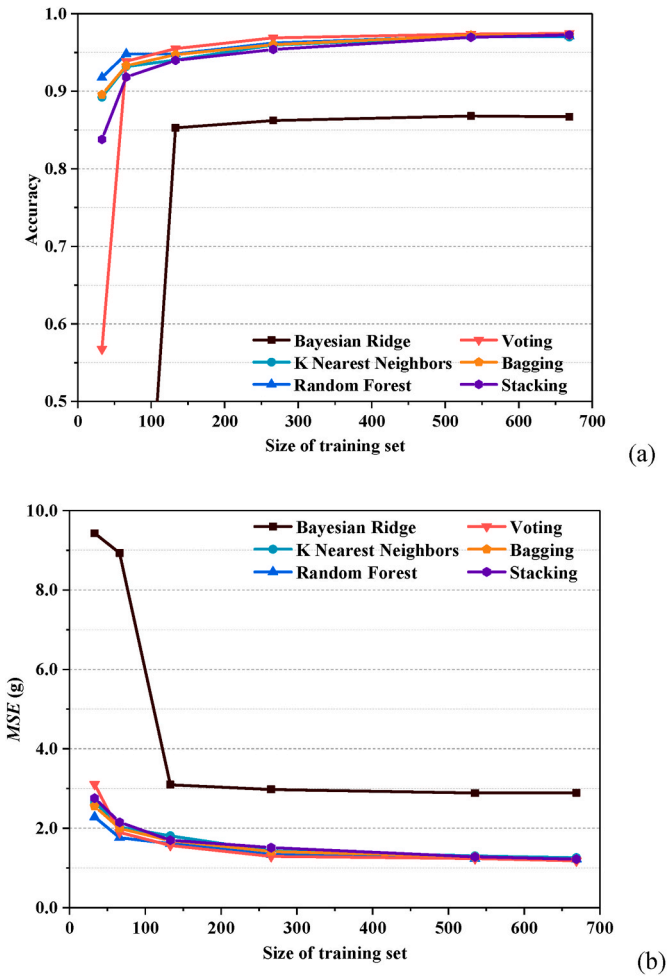

Fig. 15. The predicted performance of ML models trained by training sets with different size.
(a) Accuracy (b) MSE.

Therefore, the expansion thickness of corrosion products at the end of the test can be calculated by the above formulas and the corrosion degree ρ measured by experiments as listed in Table 6.

2.3.2. Constitutive model of rubber concrete

In this study, different constitutive models are used for different zones. The elastic constitutive model is selected for aggregates. Concrete damage plasticity (CDP) model is adopted to investigate the compressive crushing and tensile cracking behavior of rubber mortar. The thickness of interface transition zone (ITZ) is 10–50 μm, which is much smaller than the element size. Thus, cohesive element without thickness is used to simulate the behavior of ITZ. Elastic modulus and strength of the ITZ are chosen to be approximately 80% of the mortar's [53]. The selected failure criterion of cohesive element is Quadratic separation criterion as shown in the following formula:

$$\left(\frac{t_n}{t_{n0}}\right)^2+\left(\frac{t_s}{t_{s0}}\right)^2+\left(\frac{t_t}{t_{t0}}\right)^2=1 \tag{12}$$

where t_n, t_s, t_t are the normal and shear stress of cohesive element, t_{n0}, t_{s0}, t_{t0} and represent the peak values of the contact stress (normal and shear stress). The material parameters of rubber concrete are obtained by the results of mechanical experiments as detailed in Table 7.

2.3.3. Generation of real aggregate based stochastic model

To realize the generation of mesoscale model with high detailed irregular aggregate in rubber concrete, three-dimensional laser scanning technology is adopted as shown in Fig. 6 (a). The spatial distribution of aggregate in concrete is discontinuous and discrete element method can accurately characterize the motion of discontinuous medium. In this study, the scanned geometric model of aggregates is transferred to the clumps for the generation and delivery of real-shaped irregular aggregate. The generation process of irregular aggregate in rubber concrete model can be divided into the following four steps:

(1) Delivering aggregate clumps into a prism space with the size of 800mm × 400mm × 100mm according to the gradation shown in Fig. 7. The aggregate gradation of experiment and simulation are in good agreement, verifying the validity of aggregate distribution.
(2) Two rigid extrusion plates and a steel bar are arranged at the boundaries and middle in the length direction. And then the two extrusion plates are controlled extruding the aggregates inward at a uniform speed, until the aggregate clumps move into a region within 100 mm, as shown in Fig. 8.
(3) Extracting the size, position and rotation information of each aggregate as shown in Supplementary Information 3 and mapping the discrete delivered aggregates into continuous medium geometric model by the code developed by our team.
(4) Finally, discretizing the geometric model is into finite element model with structured mesh. Assigning material parameters to aggregate, mortar and ITZ according to Table 7. The 3D mesoscopic model of a rubber concrete specimen with highly detailed irregular aggregates is shown in Fig. 9.

3. Results and discussion

3.1. Results of electrochemical corrosion

Fig. 10 illustrates that the time-frequency diagrams obtained by continuous wavelet transform are quite similar. The dominant frequency of signals and the frequency distribution of specimen PC, RC10 and RC20 are shown in Fig. 10 (d). Although the dominant frequency of signals sampled from RC20 is slightly smaller than that of PC and RC10, the frequency difference of each mix proportion is only 0.795 kHz. That means the rubber content has little effect on the dominant frequency of the active ultrasonic signals.

Fig. 11 shows the changing process of current and corrosion degree of the specimen PC, RC10 and RC20. The following results can be obtained: (1) The corrosion process of steel bars consists of three stages, including current stabilized phase, current dropping phase and current rising phase. (2) With the increase of rubber content, the stable time of current (in the first stage) becomes longer. (3) The corrosion degree of reinforced rubber concrete is a monotonically increasing function of power-on time. (4) In any process, the orders of current and corrosion degree are the same, from high to low is PC > RC10 >RC20. The reason is that the addition of rubber will increase the resistivity of concrete and prevent the penetration of chloride ions. Thus, higher rubber content in concrete could reduce the corrosion effect of chloride ions on steel bars.

3.2. Prediction performance of ML models

The relationship between nondestructive results (ultrasonic testing) and corrosion degree by ML models are established. The predicted corrosion degree of six ML models tested in this study are shown in Fig. 12. Table 8 list the evaluation measures of 5-fold cross validation to avoid random errors as much as possible. By comparing the calculated corrosion degree with the predicted value, following results can be drawn: (1) There are several negative values of corrosion degree in the predicted results of BR, which is obvious incorrect; (2) All models except the linear model (BR) performs well in this regression problem; (3) The accuracy of KNN, RF, voting, bagging and stacking are quite close, with

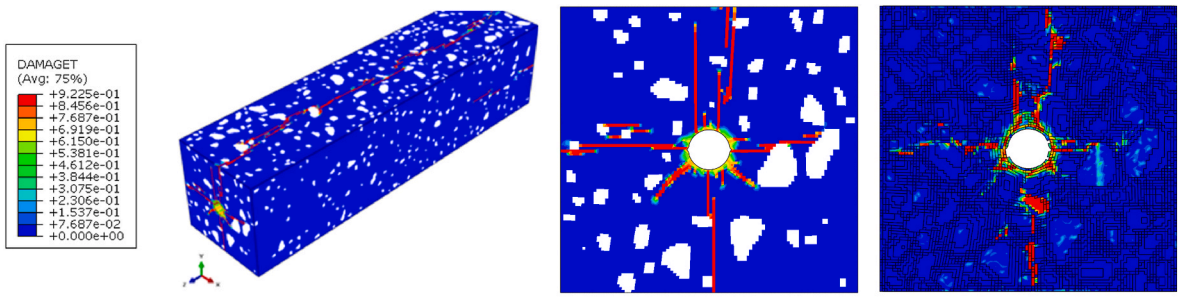

(a) PC.

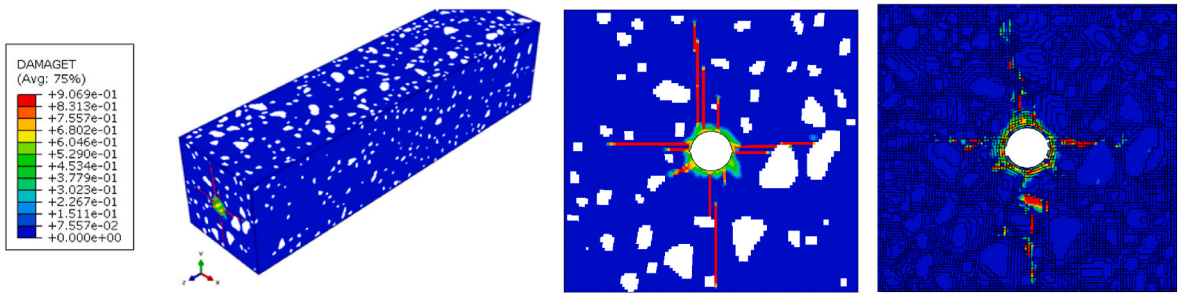

(b) RC10.

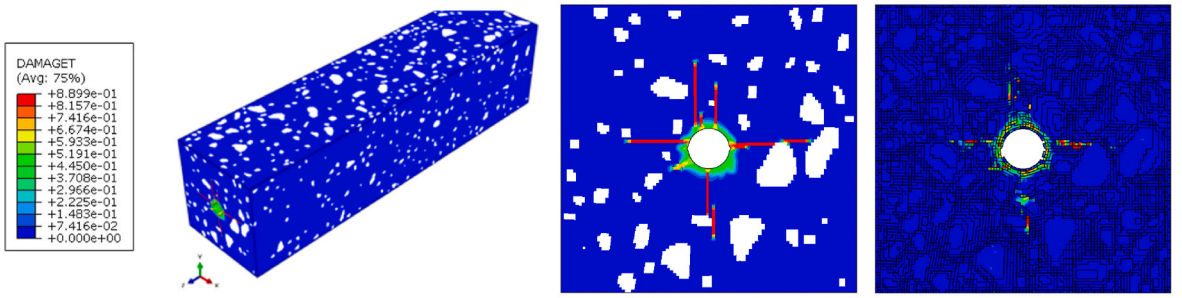

(c) RC20.

Fig. 16. Deterioration patterns of mortar and ITZ in concrete with different rubber content.

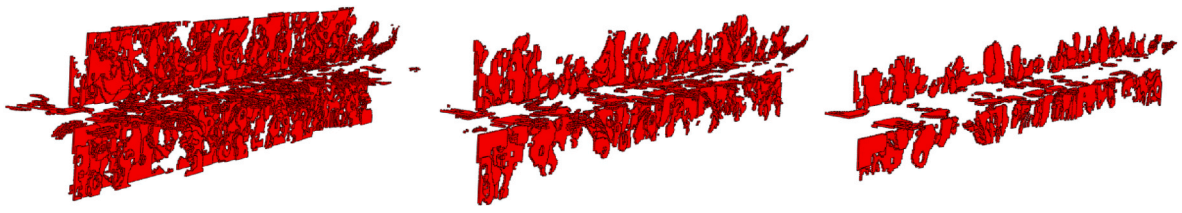

(a) PC (b) RC10 (c) RC20

Fig. 17. Tensile damage of the concrete with different rubber content.

voting performs slightly better than others; (4) The mass loss of reinforced concrete can be accurately predicted by ML models, indicating the relationship between the monitoring indicators of ultrasonic testing and corrosion degree can be expressed directly.

The input variables can be treated as several features, and they have different effects on the corrosion degree in rubber concrete. The feature importance can be generalized by its average over all of the regression trees. According to the results, ultrasonic amplitude has the greatest contribution to predict the mass loss as shown in Fig. 13. Therefore, more attention should be paid to the monitoring accuracy of ultrasonic amplitude, so as to improve the prediction performance of ML models and obtain more accurate corrosion degree of steel bars in concrete structure.

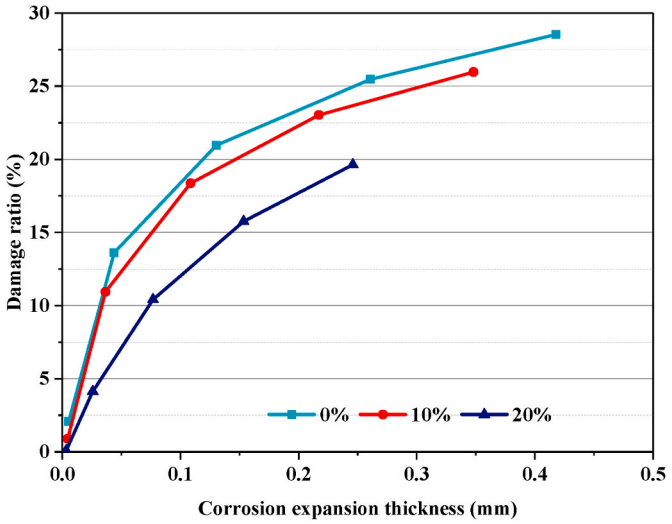

Fig. 18. The relationship between rubber concrete damage ratio and corrosion expansion thickness.

3.3. Robustness validation of prediction model

3.3.1. Abnormal ultrasonic amplitude

During the collecting process of monitoring data, the on-site conditions definitely interfere with the accuracy of collected data to varying degrees. It is an effective means to evaluate the robustness of models using the input variables, which are disturbed by outliers, to predict the corrosion degree of rebar in reinforced concrete structure. Due to the outstanding importance of ultrasonic amplitude, we add the random disturbance, whose range is [-*k*, *k*], to each original amplitude. *k* is a multiple of the original amplitudes. Fig. 14 displays the prediction accuracy changes with increasing interference. The results show that the accuracy of all models decreases with the increase of amplitude disturbance, but the accuracy of all models except the BR still maintained at a high level (around 95%) under the interference of 20% amplitude, verifying the favorable robustness of the RF model.

3.3.2. Influence of the size of training set

Generally, the prediction performance of machine learning models is directly related to the size of the training set. There may be a limited amount of data collected for the training of ML models. Thus, the size of training set in this study is reduced to 16, 33, 66, 133, 267, 399, 534 and 668, respectively. The same testing set with the size of 169 is selected for the verification of predicted models, which are trained by above training sets. Fig. 15 shows the prediction performance of ML models trained by different sizes of training sets. The results show that: (1) With the increase of training data, the accuracy increases gradually, while the mean square error (MSE) decreases. (2) When the size of the training set is greater than 66, the prediction accuracy of all models is more than 90% except Bayesian Ridge; (3) Once the size of training set exceeds 133, the voting is very prominent, and when the size is less than 133, the random forest performs best. Therefore, to a certain extent, the robustness of the ML models can overcome the limitation of training set size.

3.4. Deterioration pattern analysis of rubber concrete

Corrosion damage of reinforced concrete structures is mainly due to the excessive tensile stress caused by volume expansion of steel bars after corrosion. The addition of rubber has both positive and negative influences on the durability of reinforced concrete structures. On the one hand, rubber will hinder the transmission of chloride ions in rubber concrete structures, prevent the production of corrosion products, and further reduce the volume expansion of steel bars, which is beneficial to preventing steel bars from corrosion. On the other hand, the addition of rubber will reduce the tensile strength of rubber concrete, which is unfavorable to the durability of reinforced concrete structures. Therefore, in order to judge whether adding rubber is beneficial to improvement of the durability of structure, this study quantitatively analyzes the deterioration process of rubber concrete caused by corrosion expansion through experiments and numerical simulation.

Fig. 16 and Fig. 17 illustrates the simulation results of the deterioration pattern of concrete with rubber content of 0%, 10% and 20%. The red area represents the area where the tensile damage occurred. The results indicate that both the mortar and interface transition zone of rubber concrete are deteriorated, which is consistent with the experimental results. It can be seen that the damage gradually extends to the outer surface of rubber concrete along the holes of steel bars and finally form a set of intersecting cracks (see Fig. 18).

Fig. 18 shows the relationship between the rubber concrete damage ratio (ratio of damaged region to total region) and the corrosion expansion thickness in the numerical simulation of steel expansion induced by corrosion. It can be seen that the damage ratio of rubber concrete in the initial period increases rapidly with the increase of the corrosion thickness of the steel bar, but when the corrosion thickness reaches 0.1 mm, the increase rate of the damage ratio slows down. With the increase of rubber content, the damage area of rubber concrete gradually decreases, indicating that the incorporation of rubber can effectively reduce the damage of concrete after the corrosion and expansion of steel bars.

4. Conclusion

In this paper, the corrosion degree of RC with various rubber content was evaluated by integrating machine learning and mesoscale simulation. It provides a new nondestructive way to the evaluation of corrosion in concrete structures. The following conclusions can be drawn:

(1) According to the value of corrosion current, higher rubber content in concrete can improve the corrosion resistance and reduce the corrosion effect of chloride ions on steel bars.
(2) ML models excepted linear model can accurately predict the corrosion degree in rubber concrete, without complicated process of parameters adjustment. The excellent robustness of these models could guarantee the application prospect of the proposed idea.
(3) As a nondestructive method, ultrasonic amplitude is the most important monitoring index to evaluate the corrosion in rubber concrete. The measurement accuracy of ultrasonic amplitude needs to be guaranteed in engineering practice.
(4) The steel corrosion induced deterioration in reinforced concrete can be effectively mitigated by the incorporation of rubber, evidenced from lower damage ratios at the same steel corrosion degree.

The deterioration extent of concrete with various rubber content caused by corrosion is quantitatively evaluated. Nevertheless, the research of this paper still has some limitations. The arrangement of steel bars in rubber concrete is relatively simple. The future work will focus on the applicability of model to detect the corrosion of rubber reinforced concrete formed by steel bars of various layouts.

Declaration of competing interest

The authors declare that they have no known competing financial interests or personal relationships that could have appeared to influence the work reported in this paper.

Acknowledgments

Financial support from the National Natural Science Foundation of China under the grants of 52078332, U2006223 and 51925805, from the Natural Science Foundation of Hebei Province under the grant of E2020402079 and from the Guangdong Provincial Key Laboratory of Durability for Marine Civil Engineering (SZU) under the grant of 2020B1212060074 is gratefully acknowledged.

Appendix C. Supplementary data

Supplementary data to this article can be found online at https://doi.org/10.1016/j.cemconcomp.2022.104426.

Appendix A. Descriptions of Machine Learning Models Used in This Study

(1) Bayesian Ridge

Bayesian Ridge algorithm is a Bayesian linear regression [54], which is based on Bayesian inference [55]. In the principle of Bayesian linear regression, the parameters of the linear model are regarded as random variables, and the posterior values of parameters are calculated by using prior knowledge. It is assumed that $\boldsymbol{X} = \{x_1, x_2, \ldots, x_N\} \in \mathbf{R}^N$ and $\boldsymbol{y} = \{y_1, y_2, \ldots, y_N\}$ are the training set, then the Bayesian linear regression model is:

$$f(\mathbf{X}) = \mathbf{X}^T\mathbf{w}, \quad \mathbf{y} = f(\mathbf{X}) + \varepsilon \tag{A1}$$

where ε is the residual, $\boldsymbol{w}$ is the weights. The variance of residuals follows the inverse gamma distribution:

$$\begin{cases} p(\varepsilon) = N\left(\varepsilon|\mu_n, \sigma_n^2\right) \\ \sigma_n^2 = \text{Inv} - \text{Gamma}\left(\sigma_n^2|a, b\right) \end{cases} \tag{A2}$$

where, the mean of ε, μ_n, and (a, b) are determined by the prior knowledge. Because the $\boldsymbol{w}$ is independent of $\boldsymbol{X}$ and σ_n^2, the posterior of $\boldsymbol{w}$ can be derived formula (S3) by the Bayes' theorem.

$$p\left(\mathbf{w}|\mathbf{X}, \mathbf{y}, \sigma_n^2\right) = \frac{p\left(\mathbf{y}|\mathbf{X}, \mathbf{w}, \sigma_n^2\right)p(\mathbf{w})}{p\left(\mathbf{y}|\mathbf{X}, \sigma_n^2\right)} \tag{A3}$$

where $p(\mathbf{y}|\mathbf{X}, \mathbf{w}, \sigma_n^2)$ is the likelihood, $p(\mathbf{y}|\mathbf{X}, \sigma_n^2)$ is the marginal likelihood of $\boldsymbol{y}$, and is only related to the training set $\boldsymbol{X}$. Our goal is to maximize the likelihood. In this research, the Maximum A Posterior estimation (MAP) is used, as follows:

$$p(\mathbf{w}) = N\left(\mathbf{w}|0, \sigma_{\mathbf{w}}^2\right) \tag{A4}$$

There are four more hyperparameters, α_1, α_2, λ_1, λ_2 of the gamma prior distributions over α and λ. n_iter is the maximum number of iterations.

(2) K-Nearest Neighbors

K-Nearest Neighbors algorithm, is a relatively mature method, in theory, is also one of the simplest machine learning algorithms, supervised algorithm [56]. The idea is that a sample belongs to a category if most of the *k* most similar samples in the feature space belong to that category [57].

If each training sample is regarded as a point in n-dimensional space, all training samples can be stored in n-dimensional space. When a sample of an unknown category is given, *k* samples closest to the unknown sample are found by searching the *n*-dimensional feature space. If most of the *k* most similar (that is, the nearest neighbor in the feature space) samples of this sample belong to a certain category, then this sample also belongs to this category. Two samples $X = \{x_1, x_2, \ldots, x_n\}$ and $Y = \{y_1, y_2, \ldots, y_n\}$ is often described by Euclidean distance:

$$D(X, Y) = \sqrt{\sum_{i=1}^{n}(x_i - y_i)^2} \tag{A5}$$

The following three factors affect the *K*-Nearest Neighbors:

1) The value of *K*. The selected *K* value is large or small, and the number of samples in each category in the *K* neighborhood of the samples to be tested is also different.
2) Distance measurement. The distance between the test sample and the training sample will be affected by the distance function. The selected metric in this study is minkowski.
3) Decision rules. Different decision rules will lead to different classification scores, so the prediction results will be different.

(3) Random forest

Random forest algorithm is an integrated learning method based on a decision tree proposed by Leo Breiman and Adele Culter in 2001 [58]. It is a nonlinear modeling algorithm and can be used for classification and regression problem analysis. Among machine learning algorithms, the random forest algorithm has the advantages of high accuracy, insensitivity to multiple collinearities, and difficulty in over-fitting, and is widely used in medicine, biology, economy, and other fields [59].

The random forest regression algorithm is a model composed of a series of regression decision subtrees. The output value of the random forest regression model is the average value of the results of all decision subtrees in the random forest, which can be expressed as:

$$\overline{h}(x) = \frac{1}{T}\sum_{t=1}^{T}\{h(x,\theta_t)\} \tag{A6}$$

In this study, the number of trees in the forest is 100 and the minimum number of samples required to split an internal node is 2. The process of random forest regression algorithm is as follows: 1) Bagging idea is applied to generate the sample set of each subtree; 2) Using the idea of random subspace, *k* features are randomly selected for node splitting to construct a single regression decision subtree; 3) Repeat steps 1) and 2) to construct T regression decision subtrees and form forests; 4) Take the average predicted value of T regression decision subtree as the final result of random forest regression.

(4) Voting

The idea behind the Voting Regressor is to combine conceptually different machine learning regressors and return the average predicted values. Such a regressor can be useful for a set of equally well performing models in order to balance out their individual weaknesses. Fig. A1 shows the Voting Regressor in this study.

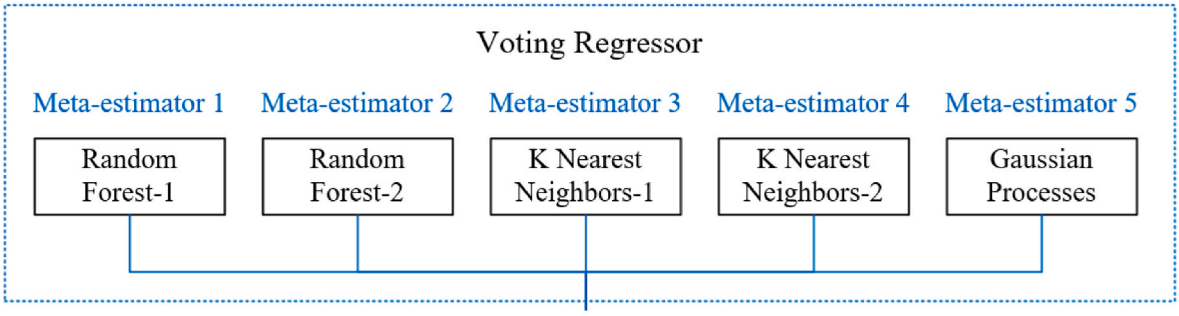

Fig. A1. Voting Regressor in this study.

(5) Bagging

In ensemble algorithms, bagging methods form a class of algorithms which build several instances of a black-box estimator on random subsets of the original training set and then aggregate their individual predictions to form a final prediction [60]. These methods are used as a method to reduce the variance of basic estimators by introducing randomization into its construction process and then integrating it. In many cases, bagging methods is a very simple method to improve a single model without modifying the underlying basic algorithm. Because they provide a method to reduce over-fitting, bagging methods works best in the strong model and complex models, which is in contrast with the enhancement methods which usually works best in the weak models.

(6) Stacking

Stacking is a method for combining estimators to reduce their biases [61]. More precisely, the predictions of each independent estimator are superimposed and used as input of the final estimator to calculate the prediction. This final estimator is trained through cross-validation. In practice, a stacking predictor predicts as well as the best predictor of the base layer and even sometimes outperforms it by combining the different strengths of these predictors. However, the computational cost of training a stack predictor is high. Fig. A2 shows the Stacking Regressor in this study.

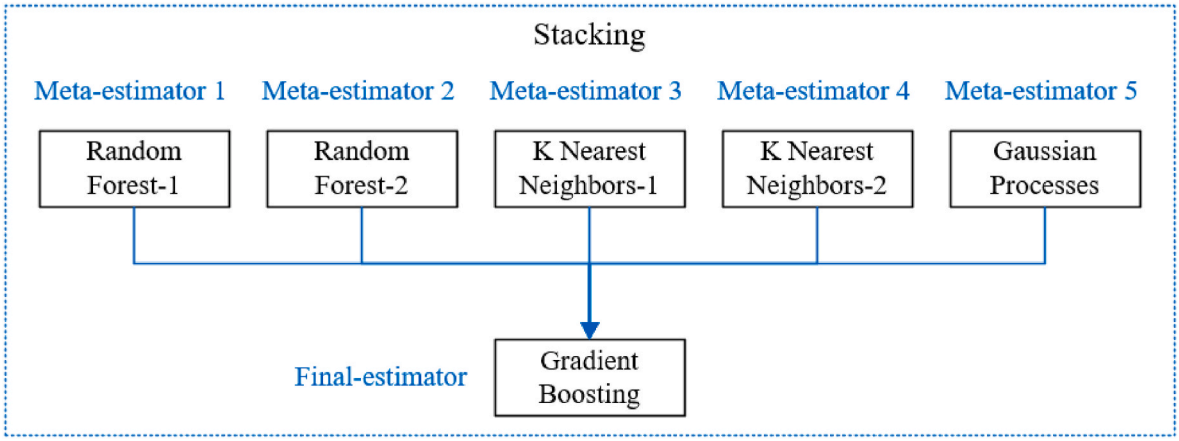

Fig. A2. Stacking Regressor in this study.

Appendix B. Computation theory of aggregate placement in This Study

In the discontinuous medium model, the aggregate "particle cluster" model contains three important information: size information, rotation information and location information. The data of each aggregate can be transmitted to the finite element model after scaling, rotation and translation.

(1) Scaling of the aggregate

The unified particle model of particles is established, and he aggregate scaling size is γ. Assuming that the coordinate before scaling is (x_0, y_0, z_0) and the coordinate after scaling is (x_1, y_1, z_1), then the new coordinate can be obtained through the following scaling transformation:

$$(x_1, y_1, z_1) = \gamma \cdot (x_0, y_0, z_0) \tag{B1}$$

(2) Rotation of the aggregate

In order to transfer the coordinate rotation of the aggregate particles to the finite element, the Euler angle transformation is carried out, and the random aggregate particle model is established in the finite element. Therefore, it is necessary to convert the quaternion to the Euler angle, which is expressed by the yaw angle rotating around the z axis φ, the pitch angle rotating around the y axis θ and the roll angle rotating around the x axis φ. The coordinate before the rotation of the aggregate is (x_1, y_1, z_1), and the coordinate after the rotation is (x_2, y_2, z_2). The expression of the quaternion is as follows:

$$Q = q_0 + q_1\mathbf{i} + q_2\mathbf{j} + q_3\mathbf{k} \tag{B2}$$

The coordinate relation of aggregate before and after rotation is:

$$\begin{bmatrix} x_2 \\ y_2 \\ z_2 \end{bmatrix} = \begin{bmatrix} q_0^2 + q_1^2 - q_2^2 - q_3^2 & 2(q_1q_2 - q_0q_3) & 2(q_0q_2 + q_1q_3) \\ 2(q_0q_3 + q_1q_2) & q_0^2 - q_1^2 + q_2^2 - q_3^2 & 2(q_2q_3 - q_0q_1) \\ 2(q_1q_3 - q_0q_2) & 2(q_0q_1 + q_2q_3) & q_0^2 - q_1^2 - q_2^2 + q_3^2 \end{bmatrix} \begin{bmatrix} x_0 \\ y_0 \\ z_0 \end{bmatrix} \tag{B3}$$

The Euler angle is used to represent the coordinate relationship before and after rotation in the order of z, y, x, as shown in formula (S4):

$$\begin{bmatrix} x_2 \\ y_2 \\ z_2 \end{bmatrix} = \begin{bmatrix} \cos\varphi\cos\theta & \sin\varphi\cos\theta & -\sin\theta \\ \cos\varphi\sin\theta\sin\varphi - \sin\varphi\cos\varphi & \sin\varphi\sin\theta\sin\varphi + \cos\varphi\cos\varphi & \cos\theta\sin\varphi \\ \cos\varphi\sin\theta\cos\varphi + \sin\varphi\sin\varphi & \sin\varphi\sin\theta\cos\varphi - \cos\varphi\sin\varphi & \cos\theta\cos\varphi \end{bmatrix} \begin{bmatrix} x_0 \\ y_0 \\ z_0 \end{bmatrix} \tag{B4}$$

Corresponding the matrix of formula (B3) and formula (B4) one by one, the calculation formula of Euler angle is obtained. The following formula shows:

$$\begin{cases} \tan\varphi = \dfrac{2(q_1q_2 - q_0q_3)}{q_0^2 + q_1^2 - q_2^2 - q_3^2} \\ \sin\theta = -2(q_0q_2 + q_1q_3) \\ \tan\varphi = \dfrac{2(q_2q_3 - q_0q_1)}{q_0^2 - q_1^2 - q_2^2 + q_3^2} \end{cases} \tag{B5}$$

when rotating in the order of z, y and x, the new coordinate axis needs to rotate in the following way: 1) The rotation angle is around the z axis, and the vector of z axis is defined as $(0, 0, 1)$ in the finite element. 2) rotate around the new y axis, where the vector of the new y axis is $(-\sin\varphi, \cos\varphi, 0)$. 3) Rotation around the new x axis, the vector of the new x axis is $(\cos\varphi\cos\theta, \sin\varphi\cos\theta, -\sin\theta)$.

(3) Translation of the aggregate

If the position information of aggregate particles in the discontinuous method is (a, b, c), and the coordinate of rotation of particles is (x_3, y_3, z_3), then the following equation should be satisfied:

$$(x_3, y_3, z_3) = (x_2 + a, y_2 + b, z_2 + c) \tag{B6}$$

References

[1] S. Sadati, M. Arezoumandi, M. Shekarchi, Long-term performance of concrete surface coatings in soil exposure of marine environments, Construct. Build. Mater. 94 (2015) 656–663.

[2] Y. Yi, D. Zhu, S. Guo, et al., A review on the deterioration and approaches to enhance the durability of concrete in the marine environment, Cement Concr. Compos. 113 (2020) 103695.

[3] A. James, E. Bazarchi, A. Chiniforush, et al., Rebar corrosion detection, protection, and rehabilitation of reinforced concrete structures in coastal environments: a review, Construct. Build. Mater. 224 (2019) 1026–1039.

[4] O. Youssf, J. Mills, T. Benn, et al., Development of crumb rubber concrete for practical application in the residential construction sector – design and processing, Construct. Build. Mater. 260 (2020) 119813.

[5] Q. Han, N. Wang, J. Zhang, et al., Experimental and computational study on chloride ion transport and corrosion inhibition mechanism of rubber concrete, Construct. Build. Mater. 268 (2021) 121105.

[6] A. Khaloo, M. Dehestani, P. Rahmatabadi, Mechanical properties of concrete containing a high volume of tire – rubber particles, Waste Manag. 28 (12) (2008) 2472–2482.

[7] C. Wang, Y. Zhang, A. Ma, Investigation into the fatigue damage process of rubberized concrete and plain concrete by AE analysis, J. Mater. Civ. Eng. 23 (7) (2011) 953–960.

[8] N. Oikonomou, S. Mavridou, Improvement of chloride ion penetration resistance in cement mortars modified with rubber from worn automobile tires, Cement Concr. Compos. 31 (6) (2009) 403–407.

[9] M. Bravo, J. de Brito, Concrete made with used tyre aggregate: durability-related performance, J. Clean. Prod. (25) (2012) 42–50.

[10] T. Liu, R. Weyers, Modeling the dynamic corrosion process in chloride contaminated concrete structures, Cement Concr. Res. 28 (3) (1998) 365–379.

[11] B. Yu, L. Yang, M. Wu, et al., Practical model for predicting corrosion rate of steel reinforcement in concrete structures, Construct. Build. Mater. (54) (2014) 385–401.

[12] A. Scott, M. Alexander, The influence of binder type, cracking and cover on corrosion rates of steel in chloride-contaminated concrete, Mag. Concr. Res. 59 (7) (2007) 495–505.

[13] B. Huet, V. L'hostis, G. Santarini, et al., Steel corrosion in concrete: determinist modeling of cathodic reaction as a function of water saturation degree, Corrosion Sci. 49 (4) (2007) 1918–1932.

[14] J. Zhang, C. Liu, M. Sun, et al., An innovative corrosion evaluation technique for reinforced concrete structures using magnetic sensors, Construct. Build. Mater. 135 (15) (2017) 68–75.
[15] S. Hong, F. Zheng, G. Shi, et al., Determination of impressed current efficiency during accelerated corrosion of reinforcement, Cement Concr. Compos. 108 (2020) 103536.
[16] S. Hong, G. Shi, F. Zheng, et al., Characterization of the corrosion profiles of reinforcement with different impressed current densities by X-ray micro-computed tomography, Cement Concr. Compos. 109 (2020) 103583.
[17] C. Andrade, J. Gonzalez, Quantitative measurement of corrosion rate of reinforcing steels embedded in concrete using polarization resistance measurements, Mater. Corros. 29 (8) (1978) 515–519.
[18] C. Andrade, C. Alonso, Corrosion rate monitoring in the laboratory and on-site, Construct. Build. Mater. 10 (5) (1996) 315–328.
[19] R. Polder, Test methods for on-site measurement of resistivity of concrete - a RILEM TC-154 technical recommendation, Construct. Build. Mater. 15 (2001) 125–131.
[20] B. Elsener, C. Andrade, J. Gulikers, et al., Half-cell potential measurements - potential mapping on reinforced concrete structures, Mater. Struct. 36 (2003) 461–471.
[21] N. Smagina, A. Trifonova, O. Bou Matar, Local damage detection by nonlinear coda wave interferometry combined with time reversal, Ultrasonics 108 (2018) 106226.
[22] N. Siddique, H. Adeli, Computational Intelligence: Synergies of Fuzzy Logic, Neural Networks and Evolutionary Computing, John Wiley & Sons, West Sussex, UK, 2013.
[23] M. Zhang, M. Li, Y. Shen, et al., Multiple mechanical properties prediction of hydraulic concrete in the form of combined damming by experimental data mining, Construct. Build. Mater. 207 (2019) 661–671.
[24] R. Cook, J. Lapeyre, H. Ma, et al., Prediction of compressive strength of concrete: critical comparison of performance of a hybrid machine learning model with standalone models, J. Mater. Civ. Eng. 31 (11) (2019) 1–15.
[25] R. Cai, T. Han, W. Liao, et al., Prediction of surface chloride concentration of marine concrete using ensemble machine learning, Cement Concr. Res. 136 (2020) 106164.
[26] J. Wang, D. Zhong, H. Adeli, et al., Smart bacteria-foraging algorithm-based customized kernel support vector regression and enhanced probabilistic neural network for compaction quality assessment and control of earth-rock dam, Expet Syst. 35 (6) (2018), e12357.
[27] S. Bai, M. Li, R. Kong, et al., Data mining approach to construction productivity prediction for cutter suction dredgers, Autom. ConStruct. 105 (2019) 102833.
[28] M. Zhang, M. Li, J. Zhang, et al., Onset detection of ultrasonic signals for the testing of concrete foundation piles by coupled continuous wavelet transform and machine learning algorithms, Adv. Eng. Inf. 43 (2020) 101034.
[29] M. Zhang, M. Li, S. Yang, et al., Isogeometric shape optimization of high RCC gravity dams with functionally graded partition structure considering hydraulic fracturing, Eng. Struct. 179 (2019) 341–352.
[30] M. Li, W. Si, S. Du, et al., Thermal deformation coordination analysis of CC-RCC combined dam structure during construction and operation periods, Eng. Struct. 213 (2020) 110587.
[31] E. Gebreyouhannes, K. Maekawa, Nonlinear gel migration in cracked concrete and broken symmetry of corrosion profiles, J. Adv. Concr. Technol. 14 (6) (2016) 271–286.
[32] V. Kuntal, P. Jiradilok, J. Bolander, et al., Estimation of internal corrosion degree from observed surface cracking of concrete using mesoscale simulation with Model Predictive Control, Comput. Aided Civ. Infrastruct. Eng. (2020) 1–16.
[33] Y. Huang, D. Yan, Z. Yang, et al., 2D and 3D homogenization and fracture analysis of concrete based on in-situ X-ray Computed Tomography images and Monte Carlo simulations, Eng. Fract. Mech. 163 (2016) 37–54.
[34] S. Yang, Z. Yang, H. Jing, et al., Fracture evolution mechanism of hollow sandstone under conventional triaxial compression by X-ray micro-CT observations and three-dimensional numerical simulations, Int. J. Solid Struct. 190 (2020) 156–180.
[35] P. Thilakarathna, K. Baduge, P. Mendis, et al., Mesoscale modelling of concrete – a review of geometry generation, placing algorithms, constitutive relations and applications, Eng. Fract. Mech. 231 (2020), 06974.
[36] R. Peng, W. Qiu, F. Teng, Three-dimensional meso-numerical simulation of heterogeneous concrete under freeze-thaw, Construct. Build. Mater. 250 (2020) 118573.
[37] W. Cui, W. Yan, H. Song, et al., DEM simulation of SCC flow in L-Box set-up: influence of coarse aggregate shape on SCC flowability, Cement Concr. Compos. 109 (2020) 103558.
[38] D. Liu, X. Xia, L. Sun, Movement and embedding characteristics of interlayer aggregates during roller-compacted concrete compaction process using discrete element simulation, Construct. Build. Mater. 249 (2020) 1–15.
[39] D. Donskoy, K. Ferroni, A. Sutin, et al., A nonlinear acoustic technique for crack and corrosion detection in reinforced concrete, Nondestruct. Character. Mater. Viii (1998) 555–560.
[40] P. Antonaci, C. Bruno, M. Scalerandi, et al., Effects of corrosion on linear and nonlinear elastic properties of reinforced concrete, Cement Concr. Res. 51 (2013) 96–103.
[41] M. Climent, M. Miró, J. Carbajo, et al., Use of non-linear ultrasonic techniques to detect cracks due to steel corrosion in reinforced concrete structures, Materials 12 (5) (2019) 813.
[42] M. Miró, J. Eiras, P. Poveda, et al., Detecting cracks due to steel corrosion in reinforced cement mortar using intermodulation generation of ultrasonic waves, Construct. Build. Mater. 286 (2021) 122915.
[43] T. Maaddawy, K. Soudki, Effectiveness of impressed current technique to simulate corrosion of steel reinforcement in concrete, J. Mater. Civ. Eng. 15 (1) (2003) 41–47.
[44] F. Du, Z. Jin, W. She, et al., Chloride ions migration and induced reinforcement corrosion in concrete with cracks: a comparative study of current acceleration and natural marine exposure, Construct. Build. Mater. 263 (2020) 120099.
[45] J. Zhang, T. Fan, H. Ma, et al., Monitoring setting and hardening of concrete by active acoustic method: effects of water-to-cement ratio and pozzolanic materials, Construct. Build. Mater. 88 (2015) 118–125.
[46] Z. Moradian, H. Einstein, G. Ballivy, Detection of cracking levels in brittle rocks by parametric analysis of the acoustic emission signals, Rock Mech. Rock Eng. 49 (3) (2016) 785–800.
[47] J. Zhang, H. Ma, W. Yan, et al., Defect detection and location in switch rails by acoustic emission and Lamb wave analysis: a feasibility study, Appl. Acoust. 105 (2016) 67–74.
[48] C. Li, B. Campbell, Y. Liu, et al., A fast multi-layer boundary element method for direct numerical simulation of sound propagation in shallow water environments, J. Comput. Phys. 392 (2019) 694–712.
[49] Scikit-learn, 2021. https://scikit-learn.org/stable/.
[50] X. Xi, S. Yang, C. Li, A non-uniform corrosion model and meso-scale fracture modelling of concrete, Cement Concr. Res. 108 (2018) 87–102.
[51] Y. Zhang, R. Su, Concrete cover delamination model for non-uniform corrosion of reinforcements, Construct. Build. Mater. 223 (2019) 329–340.
[52] X. Du, J. Liu, R. Zhang, Modeling the cracking of cover concrete due to non-uniform corrosion of reinforcement, Corrosion Sci. 89 (2014) 189–202.
[53] J. Xiao, W. Li, Z. Sun, et al., Properties of interfacial transition zones in recycled aggregate concrete tested by nanoindentation, Cement Concr. Compos. 37 (2013) 276–292.
[54] A. Chan, N. Vasconcelos, Counting people with low-level features and Bayesian regression, IEEE Trans. Image Process. 21 (2011) 2160–2177.
[55] L. Firinguetti-Limone, M. Pereira-Barahona, Bayesian estimation of the shrinkage parameter in ridge regression, Commun. Stat. Simulat. Comput. 12 (2019) 1–14.
[56] T. Cover, P. Hart, Nearest neighbor pattern classification, IEEE Trans. Inf. Theor. 13 (1967) 21–27.
[57] H. Yigit, ABC-based distance-weighted KNN algorithm, J. Exp. Theor. Artif. Intell. 27 (2015) 189–198.
[58] L. Breiman, Random forests, Mach. Learn. 45 (2001) 5–32.
[59] J. Song, Bias corrections for Random Forest in regression using residual rotation, J. Korean Surg. Soc. 44 (2015) 321–326.
[60] T. Ho, The random subspace method for constructing decision forests, IEEE Trans. Pattern Anal. Mach. Intell. 20 (8) (1998) 832–844.
[61] H. David, Stacked generalization, Neural Network. 5 (2) (1992) 241–259.